Influence of PbO Stoichiometry on the Properties of PZT Ceramics and Multilayer Actuators

Moritz Oldenkotte[1], Hans Kungl[2], Rüdiger-A. Eichel[2], Kristin A. Schönau[3], Marc Kühlein[3], Thilo Bernard[3], Michael J. Hoffmann[4] and Manuel Hinterstein[4,*]

[1]sia Abrasives Industries AG, Mühlewiesenstraße 20, CH-8501 Frauenfeld, Switzerland

[2]Institute of Energy and Climate Research: Fundamental Electrochemistry IEK-9, Forschungszentrum Jülich, Ostring 10, Jülich 52425, Germany

[3]Robert Bosch GmbH, Germany

[4]Institute of Applied Materials, Karlsruhe Institute of Technology, Haid-und-Neu Straße 7, 76131 Karlsruhe, Germany

Abstract

Lead-oxide stoichiometry of lead-zirconate-titanate (PZT) ceramics and multilayer actuators is a critical issue for fabrication and performance. During sintering, the high vapor pressure and the corresponding volatility of lead oxide (PbO) require a careful design of sintering setup and parameters, as both may significantly impact on the PbO content in ceramics and devices. In order to investigate the effects of PbO stoichiometry, PZT compositions with different PbO contents have been synthesized and were sintered under varying temperature conditions and sintering setups. Structure and microstructure of the material was characterized using X-ray diffraction and scanning electron microscopy (SEM). Dielectric properties and high field strain

behavior were analyzed with respect to their relation to PbO content and grain size. Corresponding experiments with multilayer actuators were carried out, whereby the PbO content was varied by controlling the sintering atmosphere. The results indicate that there is a pronounced correlation between PbO content, structure and high field strain in both, PZT ceramics and multilayer actuators.

*Corresponding author. Tel.: +49 721 608 44373, Fax: +49 721 608 48891

Email address: manuel.hinterstein@kit.edu

1. Introduction

Lead oxide (PbO) stoichiometry in lead zirconate titanate (PZT) ceramics has been an issue ever since the development of devices based on this type of material started in the late 50s after filing the patents for PZT 5A and PZT 5H(1). However, the context and the point of view from which this topic has been approached have been subject to changes along with technical progress in processing of PZT materials and development of multilayer and co-firing technology of PZT based devices. While process oriented approaches established detailed knowledge on the effects on sintering behavior and lead losses(2–5), information on defect chemistry is scarce and in many cases related to the high temperature state of PZT(6,7). Work on the impact of PbO stoichiometry on macroscopic properties does not show an unequivocal trend which may serve as a guideline for process design.

The standard powder preparation in the 60s used raw materials of several microns in particle size and ball milling(8). In order to densify these materials, sintering temperatures of more than 1200°C had to be applied. The vapor pressure of PbO is increasing with Zr-content in the

solid solution(9). In this temperature range atmospheric powder had to be added to the sintering batches in order to prevent evaporation and local decomposition of PZT into its vapor form of PbO and solid ZrO_2.

Based on thermodynamic considerations, a sophisticated buffering system, consisting of a mixture of $PbZrO_3$ and ZrO_2, was designed by Holman and Fulrath(2,10) as well as Kingon and Clarke(3). Although originally derived for undoped PZT, the system works well for doped PZT materials with moderate dopant content(11). Along with the technological development of raw materials technology and the introduction of high energy ball milling, calcination temperatures could be decreased and PZT powders in or close to the submicron range became technological standard(12). This development on the one hand occurred as a spin off to meet the demand pull of emerging multilayer technology for $BaTiO_3$ based capacitors(13). On the other hand it gave rise to push application of multilayer co-firing technology also in PZT actuators(14,15).

For actuators this technology is crucial, as it enables the fabrication of thin PZT layers in multilayer technology and thus the application of high electric fields at moderate voltages. However, for application of multilayer technology, the sintering temperatures had to be reduced in order to allow for the co-firing of electrode materials with melting points limiting the sintering temperatures to less than 1100°C(14,16). Below this temperature technically reliable AgPd with economically still affordable composition of the alloy could be used. A large part of the densification in this temperature range happens due to grain boundary film sintering(14). At these lower temperatures, the lead evaporation in appropriately prepared PZT powders can be reduced to a level, which is less than the excess PbO added to promote sintering.

In optimized laboratory scale furnaces, the lead evaporation can be precisely controlled for PZT ceramics as well as for PZT films(17). In the first decade of the 21st century with the introduction of actuators for automotive fuel injection systems the mass production of actuators led to an upscaling of the sintering batches to hundreds of kilograms per batch. Keeping the atmospheric conditions and the temperature distribution constant and continuous through industrial type furnaces is still a challenge for technology. However, these are preconditions for constant PbO evaporation.

Limiting the fluctuation of PbO content has to keep pace with the narrowing of tolerances in the technological specifications on performance and characteristics of actuators. Consequently, the effects of small changes of PbO content on the performance of PZT ceramics and multilayer actuators are a major point of interest.

Lead vacancies are commonly considered to be the microscopic origin of high strain and soft electromechanical behavior in PZT(18,19). In undoped PZT the defect structure is governed by intrinsic vacancies. The intrinsic vacancies are subject to changes in PbO stoichiometry, PbO vapor pressure, sintering temperature and oxygen partial pressure of the batch composition(6,20). In donor doped PZT or co-doped PZT with donor excess, a large part of the vacancies are extrinsic ones. The existence of extrinsic vacancies mainly originates from the requirement of charge balance of aliovalent dopant ions. As long as no change in the charge compensation mechanism occurs, the extrinsic vacancy concentrations will maintain the overall level induced by the dopants. Thus, the overall effects from PbO content on vacancy concentrations are expected to be less pronounced in the doped materials. Nevertheless, changes in vacancy concentrations may significantly contribute to changes in materials properties.

However, the present paper is mainly concerned with another mechanism of influence of the PbO stoichiometry in PZT, induced by PbO excess or deficit. Paying special attention to the implications from analysis of PbO-ZrO_2-TiO_2 phase diagrams(21,22), the effects of PbO stoichiometry are traced via their effects on structural changes and variation of piezoelectric properties.

A wide range of PbO content variations within PZT-SKN ceramics was prepared. Corresponding to these materials, actuators made-up of a commercial tape-casted soft PZT comparable material composition were sintered with setups that provide different amounts of PbO losses during sintering. Ceramics and actuators were analyzed with respect to the effects of PbO content by X-ray diffraction, scanning electron microscopy, dielectric measurements and high field strain. The results indicate, that there is substantial influence of PbO content on structure, which in turn has a pronounced impact on the dielectric and electromechanical properties. The changes in structure are related to changes in Zr/Ti ratio in the PZT matrix induced by PbO excess or deficit.

2. Experimental

2.1 PZT SKN ceramics with varying PbO content in their batch compositions

PZT materials with Zr/Ti ratios 53/47 doped with 2 mol% Sr, 1.5 mol% Nb and 0.5 mol% K(23) were prepared following a mixed oxide route(12). The composition can be written either as PZT with dopant concentration such as $0.98Pb_{1+x}(Zr_{0.53}Ti_{0.47})O_3$-$0.02Sr(K_{0.25}Nb_{0.75})O_3$, or when the charge compensation through Pb vacancies V''_{Pb} is considered the full stoichiometry can be written as $Pb_{0.9675+x}Sr_{0.020}K_{0.0050}(Zr_{0.5220}Ti_{0.4630}Nb_{0.0150})O_3$. The samples were prepared with different PbO content, resulting in x ranging from -0.02 to 0.02. The powder mixtures were attrition milled in isopropanol using a polyamide crucible, a polyamide stirrer and 2 mm diameter

YTZ milling balls. After separating the slurries from the milling balls, they were dried in a rotation evaporator and stored under dry conditions for two days. Then the powder mixtures were sieved and calcined in closed alumina crucibles at 850°C for 2 h. The calcined powders were milled in polyamide crucibles using 10 mm diameter YTZ milling balls in a planetary ball mill for 6 h at 200 rpm, dried and finally sieved with 160 µm mesh metal sieves. Cylindrical pellets of 4.25 g with diameters of 10-11 mm and heights of 8-9 mm were made up by dry forming, encompassing uniaxial dye pressing and subsequent cold isostatic pressing at 500 MPa. These green bodies were stored for 1 week at 100°C under vacuum conditions before sintering them in closed alumina crucibles at 1050°C/6 h in air. For all samples mass losses during sintering were monitored by their weights, immediately before and after sintering. Densities after sintering were determined for three pellets of each composition by the Archimedes method.

For the X-ray transmission measurements thin slices from the inner part of the sintered bodies were cut and polished to 0.18 mm thickness. The samples for the electromechanical measurements were prepared by sawing slices of 1.5 mm thickness, thereafter grinding and polishing them to 1.1 mm and finally firing silver paint electrodes (Gwent C80415D5) at 600°C. The microstructures of the ceramics were analyzed from SEM images recorded from their polished surfaces after chemical etching in a H_2O-HCl-HF solution. Evaluation of structural characteristics of the PZT ceramics is based on X-ray diffraction patterns recorded at the X04SA: Materials Science beamline of the SLS in Villigen, Switzerland(24), operated at 28 keV (λ = 0.44304 Å) in transmission and recorded by the MYTHEN detector(25).

Dielectric behavior was analyzed under electric fields of 1 V/mm over a frequency range from 0.05 mHz to 1 MHz. The high frequency data were measured and recorded by means of a HP 4284 whereas for the low frequency measurements a setup combining a lock-in amplifier

(Stanford) and a charge amplifier (Kistler) was used. After poling by bipolar cycles to a maximum field of 3 kV/mm at 0.01 Hz, high field strain and polarization were measured by subsequent unipolar cycles to 2 kV/mm in custom made equipment(26,27), based on an inductive position sensor (LVDT) for the strain and a Sawyer Tower circuit for the polarization measurement.

2.2 Multilayer Actuators sintered with different sintering setups

The actuators are made-up of a commercial tape-casted soft PZT-SKN with comparable material composition to the bulk ceramics (28) and were set up in block technique. Several hundreds of layers of tape were screen printed with inner electrodes, using a Ag/Pd paste, dried and stacked to a block. The layout of the actuator is generated by a single printing layout, which is rotated every second layer by 180°, so that the electrode attaches alternating opposite surfaces of the actuator. On top and bottom of each actuator several blank layers without inner electrodes act as insulator to the front surface. Before sintering, the binder is removed during an additional heat treatment. The specimens where carefully weighted in the brown stage after de-bindering(29). Before sintering, they were stored in a climate cabinet at 30°C with 30 % relative humidity in order to avoid bias in mass losses due to moisture.

The sintering of the actuators was conducted with the intention of a wide variation of the sintering atmosphere on a laboratory scale. This was firstly implemented by varying the stocking rate within the sintering crucible between one and four actuators per sinter run and secondly by an increasing PbO pre-contamination of the crucibles. Two types of sintering setups were used, each consisting of an alumina crucible with lid and with an additional alumina framework that secured the actuator in a vertical position within the crucible (Figure 1). The

alumina framework was prepared by means of a commercial porous alumina substrate (Rubalit®708S, CeramTec GmbH, Marktredwitz). In the first type of setup the crucible was loaded with one actuator per sintering run (Figure 1a). Starting with a non-pre-contaminated crucible, seven actuators were sintered one after another, thus facing an increasing state of PbO contamination with the number of the sintering runs. In the second type of setup a crucible pre-contaminated with PbO was loaded with four actuators per sintering run, also using the crucible and alumina framework several times (Figure 1b). The temperature profile consists of a heating rate of 2.8 K/min from room temperature to 550°C, followed by a dwell time of 4 h to guarantee an even heat distribution. The maximum temperature of 1030°C is reached with a heating rate of 4.7 K/min and held for 6 h. After sintering the batch is cooled down to room temperature. The same types of sintering experiments were also applied to laminated stacks without electrodes.

The mass loss, which is an indicator for the remaining PbO content, was evaluated by weighing the specimens before and after sintering. The relative mass loss Δm/mo was calculated by dividing the weight difference before and after sintering through the initial brown state weight. The grain size was measured for two actuators, one of each sintering setup with one or four specimens per crucible. The preparation for the measurement consisted of grinding down approximately half of the actuator orthogonal to the electrodes with subsequent polishing and etching with an HF-Solution. Three pictures were taken with an optical microscope (Axio Imager M1, Carl Zeiss MicroImager GmbH, Jena, Germany) at the top, middle and end of each actuator along the axial centerline of the polished surface. Two of each three pictures were analyzed with a semi-automated software AxioVision (Steinbeis-Transferzentrum, Aalen, Germany). The d_{ci} value represents the surface weighted average of more than 4000 evaluated grains, so that sufficient statistics are ensured.

Before poling and electrical characterization the firing skin of the specimens were removed by a grinding process. Afterwards the alternating electrodes of the multilayer were connected with external Ag-Pd electrodes. The poling was performed by setting an electrical field of 0.4 kV/mm, while cooling down from an initial temperature of around 400°C. The dielectric permittivity and the dielectric loss tanδ were measured before and after poling with an LCR-meter (Agilent 4263 LCR-meter, Agilent Technologies Inc., Santa Clara) at 10 V/mm and 1 kHz. Between poling and electrical characterization, the specimens were aged for at least 24 h in dry air. The displacement of the actuators was measured with laser interferometer based equipment. The measurement took place with a signal strength of 2.3 kV/mm on the actuators, pre-stressed with 15.9(2) MPa. The signal consists of 25 pulses of 1 ms, whereas the final five ones are evaluated for the measurement.

3 Results

3.1 PZT SKN ceramic with varying PbO content in their batch compositions

Sintering at 1050°C/6 h results only in slight differences in densities of the ceramics, depending on their PbO content (Table 1). Also the grain size for all ceramics was similar with 1.2 µm as illustrated by SEM micrographs of PZT-SKN with 2 mol% PbO deficit and 2 mol% PbO excess (

Figure 2). However, significant differences were detected with respect to structural characteristics, dielectric properties and electric field induced strain. X-ray diffraction patterns, characterizing the PZT structure and the secondary phase content are shown in

Figure 3a-c. In the ceramics with PbO deficit the diffraction pattern indicates a predominantly tetragonal structure. A large part of the 200 reflections can be attributed to the tetragonal *P4mm* phase of PZT with a small amount of diffuse intensity in between (

Figure 3c). With increasing PbO content the intensity in between the tetragonal 002 and 200 reflections becomes much stronger, indicating that these ceramics contain a considerable volume fraction of material, different from the tetragonal microdomain type, i.e. nanostructured,

monoclinic or rhombohedral structure(30–32). With PbO excess a distinct third reflection is resolved, which indicates the presence of rhombohedral microdomains within the material.

Diffraction patterns in the angular range from 2θ = 7.5° to 10.0° reveal the secondary phase formation depending on the PbO content. While for the ceramics with PbO excess the presence of lead oxide modifications (e.g. litharge, 2θ = 8.16°, 8.26° and 9.05°) is detected, for the material with PbO deficit the peaks at 2θ = 8.05° indicate the presence of zirconia.

Figure 4 depicts the relative permittivity and dielectric loss in the unpoled state (ε_{up} and $\tan\delta_{up}$) and after poling (ε_{33} and $\tan\delta_{p}$). The relative permittivity in the unpoled state at 1 kHz is moderately increasing from ε_{up} = 1232 to ε_{up} = 1296 with PbO content decreasing from 2 mol% PbO excess to 2 mol% PbO deficit. The dielectric losses increase with PbO content from $\tan\delta_{up}$ = 0.020 to 0.025. Qualitatively the same trend holds over a broad frequency range from 0.05 mHz up to 1 MHz (

Figure 4). After poling, the differences in relative permittivity become much more pronounced, amounting to ε_{33} = 1747 for the ceramics with 2 mol% deficit, while remaining almost the same as in unpoled state for the composition with 2 mol% PbO excess. Dielectric losses decrease after poling by a similar extent ($\Delta\tan\delta_{p}$ = 0.005) for all materials compared to the unpoled state.

This is in agreement with observations of the permittivity as a function of composition(19). Since the diffraction patterns in

Figure 3c) appear as if a variation of PbO content is similar to a change in Zr/Ti ratio, the trend for the permittivity also appears as if the Zr/Ti ratio is changed in the same way.

Both remanent strain and unipolar strain show a characteristic but different dependence on PbO content (

Figure 5). The remanent strain is highest after applying a bipolar cycle with maximum field of 3 kV/mm for the stoichiometric PZT SKN, amounting to S_{rem} = 0.32%. With 2 mol% PbO excess

as well as with 2 mol% PbO deficit the remanent strain decreases by approximately 0.1 % compared to the stoichiometric material. In contrast to the remanent strain S_{rem}, the unipolar field induced strain S_E under 2 kV/mm shows its maximum values for PZT SKN ceramics with 1 mol% PbO deficit (S_E = 0.132 %). While towards PZT-SKN with higher PbO-deficit (2 mol%) there is moderate reduction in S_E, an increase in PbO content leads to a pronounced decrease in strain with only 0.10 % for the ceramics with 2 mol% PbO excess.

3.2 Multilayer Actuators sintered with different sintering setups

The mass losses of the multilayer actuators during sintering with the different sintering setups are shown for 10 sintering runs (7 subsequent runs with one actuator per capsule (Figure 1a), 3 subsequent runs with 4 actuators per capsule (Figure 1b)) in

Figure 6. When loaded with one actuator per sintering run, mass losses amount to 1.20 wt. % during the first sintering batch (

Figure 6, blue). Owing to the increasing degree of lead contamination of the crucible, concomitant to the number of sintering runs, the mass losses decrease in this type of setup to 0.79 wt. % for sintering run 6. Sintering run 7 showed a slightly higher sintering mass loss of 0.84 wt. %. The mass losses for the arrangement containing four multilayer actuators per batch are significantly lower, ranging from 0.97 to 0.53 wt. % (

Figure 6, red).

A quantitative evaluation of the microstructure of two actuators with significant differences in sintering mass losses is depicted in

Figure 7. The PbO content via image analysis indicates, that differences in sintering mass losses do not result in major differences in grain size (

Figure 7a and b). Equivalent grain size of 2.86 µm was calculated for an actuator sintered in the single actuator setup with 1.06 wt. % mass loss, whereas for the actuator sintered along with 4 actuator arrangement with 0.64 wt. % mass loss, a grain size of 2.90 µm was evaluated.

Permittivity and dielectric loss of the multilayer actuators after poling also show correlations to the sintering mass loss, although there is some scattering in the data (

Figure 8). The actuators with high sintering mass loss exhibit high permittivities and low dielectric loss tanδ. The actuators with reduced sintering mass loss show lower permittivities, but an increase in dielectric loss tanδ.

A significant influence of the sintering mass loss on high field displacement at 2.3 kV/mm was measured (

Figure 9). The strain of actuators subject to the highest sintering mass loss (Δm/mo = 1.2%) amounts to 0.182% and is significantly higher than for the actuator with the lowest sintering mass loss (Δm/mo = 0.6%) which yields 0.172%. The experimental series of strain measurements of actuators with different sintering mass loss establishes a clear correlation between the high field strain and the sintering mass loss.

4. Discussion

4.1 PZT SKN ceramics

Major determinants for the piezoelectric properties of ferroelectric materials are their defect structure, their microstructure and their crystallographic characteristics. The high strain of the $0.98Pb_{1+x}(Zr_{0.53}Ti_{0.47})O_3$-$0.02Sr(K_{0.25}Nb_{0.75})O_3$ ceramic is achieved by its morphotropic composition and co-doping with Sr, K and Nb. This so called PZT-SKN reaches strain up to 2 % and is well suited for high strain applications(23,33). Following textbook ideas, dopand-induced soft piezoelectric behavior can be attributed to the presence of lead vacancies(18). In PZT-SKN Sr^{2+} and K^{1+} ions substitute for Pb^{2+} on A-sites in the perovskite lattice and Nb^{5+} ions replace a Zr^{4+}/Ti^{4+} on B-sites. Nb^{5+} acts as a donor whereby its additional charges are compensated by lead vacancies V''_{Pb}. Sr^{2+}-doping lowers the Curie temperature and raises d_{33} and permittivity at ambient temperatures(33).

The charge compensation of the K^{1+} dopant may occur by oxygen vacancies $V_O^{\circ\circ}$, as suggested for the case of exclusive acceptor doping(18). Considering the results on defect dipole formation for B-site acceptors(34,35), it is however by no means clear, if formation of $V_O^{\circ\circ}$ is the only effect of acceptor A-site doping by K^{1+}. Moreover, in the case of co-doping, it is an open question if lead- and oxygen vacancies form independently or if they may recombine with lead vacancies(35,36). Depending on assumptions on charge compensation, the dopant induced lead vacancy content in PZT-SKN can be calculated from 0.75 mol% to 0.5 mol%. Compared to the dopant induced extrinsic defects, the changes in intrinsic vacancies, induced by the variation in PbO content, might be relatively small. Nevertheless, significant effects from varying PbO content on vacancy concentrations and on the properties of the PZT-SKN may be present. The experimental tools available for this work however did not include devices suitable to analyze vacancy concentrations. The following discussion therefore focusses on structural and chemical mechanisms, pointing out correlation to electromechanical properties without claiming irrelevance of additional effects from changes in defect chemistry.

Grain size has been identified to be an important determinant for piezoelectric properties(23,37–39). Mechanisms based on qualitative changes in domain patterns, grain boundary regions and clamping effects have been discussed. Moreover, the grain size induces changes in structure and/or domain configuration. In the PZT-SKN ceramics the grain size does not vary much and no systematic changes with PbO-content were detected. Although trends with PbO content cannot be completely excluded, they are below the measurable detection limits within the scattering of the data for grain size. A major influence from PbO content on grain size in the ceramic materials does not seem very probable.

However, significant differences between the materials with low and high PbO content were found with respect to their structure. With increasing PbO content the crystallographic phase content is subject to changes with increasing nanostructured and/or rhombohedral

phase content. Concomitant to the shift in phase composition, there are changes in the type and content of secondary phases. At low PbO content a secondary zirconia phase can be identified, whereas along with PbO excess higher than one mol%, PbO peaks are emerging in the diffraction patterns. These results from X-ray diffraction can be rationalized in a way that the chemical composition of the PZT material is subject to changes in Zr/Ti ratio with PbO content. The changes in structure of PZT and change in secondary phase type and content are depicted in

Figure 10.

Nominally all materials have the batch compositions with Zr/Ti ratios of 53/47. The structure of the PZT-SKN ceramics with stoichiometric composition contains tetragonal and also a significant fraction of nano- or rhombohedral domains, typical for the phase composition of PZT from the tetragonal side very close to MPB. No secondary phases are detected by X-ray diffraction. In the ceramics with PbO deficit however, the Zr partly segregates in form of secondary phase ZrO_2. This leads to a reduction of the Zr-content in the PZT material and a shift of the PZT composition toward a more Ti-rich material. Corresponding to the phase diagram, its structure tends to be more tetragonal.

On the other hand, in PZT-SKN ceramics with PbO excess, a PbO secondary phase can be detected. According to the PbO - TiO_2 - ZrO_2 phase diagram, PbO tends to dissolve substantial amounts of TiO_2, whereas the solubility for ZrO_2 is low(22). Consequently, it can be expected, that secondary phase PbO will draw Ti from the PZT matrix, thus leading to a Zr/Ti ratio higher than the nominal composition in the PZT matrix. Increasing the Zr content however implies an enhanced fraction of rhombohedral phase. This hypothesis on the effects of the PbO content can be summarized in a qualitative diagram (

Figure 10). With increasing PbO content in the ceramics, the composition of the PZT matrix is shifted to higher Zr/Ti ratio and consequently to more rhombohedral structural characteristics. Similar shift in phase composition with PbO content – although at much higher excess PbO – has been observed by Kakegawa *et al.*(40) in 1995.

Data further supporting the structural differences are provided when evaluating the dielectric data with respect to the changes in permittivity induced by poling (

Figure 11). The ratio of $\varepsilon_{33}/\varepsilon_{up}$ for the PZT-SKN ceramics with different PbO content are plotted in

Figure 11c. For PZT-SKN with PbO deficit, the permittivity increases significantly with poling, whereas for PZT-SKN with 2 mol% PbO excess it remains almost constant after poling. This implies that $\varepsilon_{33}/\varepsilon_{up}$ is significantly higher for PbO excess than for PbO deficit ceramics and close to unity for the 2 mol% PbO excess PZT.

Although there is no compound theory for an explanation of this phenomenon, experimental results for different types of ferroelectrics - PZT(19,41), KNN-LT(42) and relaxor ferroelectric PNN-PZT(43) - indicate that there is a reliable correlation between structure and the qualitative change in permittivity between unpoled and poled state. While for tetragonal materials the relation $\varepsilon_{33}/\varepsilon_{up}$ in general is larger than unity, in rhombohedral or orthorhombic structure $\varepsilon_{33}/\varepsilon_{up}$ is typically less than unity (19,41–43). Transferring this empirical correlation to the present PZT-SKN materials, the results agree well with the conclusions drawn from the diffraction patterns with respect to the shift in phase composition with PbO content.

According to the analysis of X-ray diffraction patterns, a shift in chemical composition, i.e. to Zr-rich PZT matrix in the PbO excess PZT and toward a Ti-rich PZT matrix in the PbO deficit PZT was identified as the origin of the different properties. Therefore, a qualitative comparison between the results on high field strain on PZT-SKN with fixed Zr/Ti ratio and varying PbO-content vs. PZT (LaSr-doped) with varying in Zr/Ti ratio under fixed PbO content(44) can be addressed. Typical features for the dependence of remanent strain and high field unipolar strain of morphotropic PZT materials on Zr/Ti ratio(23,26,44) are:

(i) Unipolar strain S_E shows maximum values for PZT with compositions on the tetragonal side close to the MPB, containing tetragonal phase fractions of 60% to 75%.

(ii) A significant decrease of unipolar strain for PZT at almost morphotropic compositions (<50% tetragonal) and rhombohedral materials.

(iii) Remanent strain maximum for PZT close to the MPB.

(iv) Decrease of remanent strain S_{rem} for PZT with enhanced tetragonal phase content.

High field strain data for S_E and S_{rem} typical for soft doped PZT, varying in Zr/Ti ratio and the data for PZT-SKN xPbO are opposed in

Figure 12. The high field remanent strain and high field unipolar strain in PZT-SKN 53/47 with varying PbO-content show the same features with respect to characteristic (i) – (iv) as in soft (LaSr) doped stoichiometric PZT materials with varying Zr/Ti ratio.

The effects of PbO weight losses on the dielectric constants ε_{33} and electromechanical coupling factors k_p of tetragonal and rhombohedral PZT ceramics had been subject of a study published by Webster *et al.*(45) in 1967. They found a decrease of permittivity and electromechanical coupling factors at higher PbO weight losses in tetragonal PZT ceramics, whereas for rhombohedral PZT both ε_{33} and k_p were increasing. Enhanced weight losses result in a lower effective Zr/Ti ratio in the PZT matrix via the TiO_2 dissolution mechanism, i.e. the tetragonal PZT composition "moves away from the MPB". Consequently, with maxima for permittivity and coupling factors expected at the MPB, this results in lower permittivity and electromechanical coupling factors. In contrast to that, in rhombohedral PZT, the decrease in Zr/Ti ratio owing to high PbO weight losses drives the effective composition of the matrix towards the MPB, which is favorable for both high dielectric and electromechanical properties.

4.2 Multilayer Actuators

Sintering modification experiments of the actuators cover mass losses from 0.6 to 1.2 wt.%, which roughly corresponds to PbO losses of 0.9 to 1.7 mol%. The stoichiometry of the materials in the actuators after sintering therefore ranges from slight to distinct PbO excess.

Permittivity, dielectric losses and high field strain of the multilayer actuators indicate trends for their dependence on PbO content, but are also subject to some scattering. Therefore, attempts were made to quantify these correlations to the sintering mass losses. Least square linear fits were applied to the data for permittivity in poled state, tanδ in poled state and displacement of the actuator under 2.3 kV/mm vs. the data for the sintering mass losses, each. Permittivities are positively correlated to sintering mass losses (

Figure 8a). The coefficient correlating dielectric losses tanδ with sintering mass losses is negative (

Figure 8b). Fitting parameters and correlation coefficients are summarized in Table 2. Most significant is the fact that the data for the displacement under electric field vs. the sintering mass losses are positively linked (

Figure 9) and seem to establish a very stable relationship with a high correlation coefficient of

$\rho = 0.92$ (Table 2). This means, that high mass losses during sintering are favorable for high

strain in the multilayer actuators.

4.3 Similarity and Differences between Multilayer Actuators and Ceramics

PZT-SKN ceramics and multilayer actuators show qualitatively many similarities with respect to their dependence of microstructure, structure, dielectric characteristics and strain behavior on PbO stoichiometry. Quantitatively the effects are much more pronounced in the PZT-SKN ceramics with varying batch compositions than in the actuators with PbO content variation by modifications in the sintering setup.

First, the most obvious reason for the much wider variation in dielectrical properties and strain of bulk ceramics is the stronger variation in the PbO content in the ceramics compared with the actuators. Hereby the relevant figure is the final PbO content after sintering, which can be re-calculated by subtracting mass losses from the initial batch compositions. The real PbO-contents in the bulk ceramics amount from -2.09 mol% deficit for the PZT-SKN with initially 2 mol% PbO deficit to +0.75 mol% excess for the PZT-SKN with 2 mol% PbO excess batch composition (Table 3). The real PbO-content in the actuators varies from +0.25 mol% to +1.23

mol%, hence much less. Comparison of actuator and ceramics with similar “real” PbO content indicate, that the changes within this limited range of PbO variation are not too much different. However, this does not necessarily mean that the sintered materials in ceramics and actuators, even if also their compositions are nominally the same, are identical from a materials science point of view.

A significant difference between the materials in ceramics and actuators is the grain size, amounting to 3 µm in the actuators which is almost twice as much as in the ceramics. While part of the larger grain size might be due to differences in processing of actuators and ceramics, most probably a large part of the enhanced grain growth can be attributed to diffusion of silver from electrode material during co-firing. Increasing the acceptor content, as happening when silver is substituting on the perovskite A-site in PZT ceramics, leads to enhancement of grain growth(16,46). Therefore, for a quantitative assessment on the correlation between structure and PbO content, the effects from silver diffusion and substitution in the PZT-SKN matrix had to be taken into account. In addition to the differences between ceramics and actuators with respect to PZT materials characteristics, the differences in poling procedures will influence the dielectric properties and strain. While the ceramics were poled by field cycling at ambient temperature, the actuators were subject to an industrially applied poling process, which may result in quantitative differences(47).

Dielectric data for an electrode free laminated stack indicate similar trends as for the ceramics and the actuators. Ceramics with low PbO content and stacks with high mass losses show a significant increase in permittivity after poling, whereas for ceramics with high PbO content and stacks with low sintering mass losses there are only slight poling induced changes in permittivity. Relative changes in high field strain for ceramics and actuators also show similar behavior along with excess PbO-content. Both types of samples exhibit a uniform increase of

the normalized high field strain with decreasing PbO-content. However, one has to take in account, that the absolute values of high field strain for the actuators, which vary from 0.171% to 0.182% are much higher compared to the bulk ceramics with variation from 0.112% to 0.134%. This can also be explained by the influence of different grain size(23,38). Overall, the trends in dielectric behavior and strain characteristics with respect to their dependence on PbO content are qualitatively very similar for ceramics and actuators; whereas quantitatively the levels for dielectric properties and strain as well as the effects of varying PbO content are different.

5. Conclusions

PbO stoichiometry in PZT-SKN ceramics and multilayer actuators was analyzed with respect to its influence on structure, microstructure and dielectric and ferroelectric characteristics. The PbO stoichiometry in the ceramics was varied by different PbO content in the batch compositions, whereas in multilayer actuators varied by controlling the PbO evaporation during sintering via modifications in the sintering setup. In both, ceramics and multilayer actuators, no major changes in grain size with PbO content were indicated when sintered at 1030°C-1050°C in closed crucibles under non-perturbed atmosphere.

Significant effects of the PbO content were detected by X-ray diffraction. Increasing PbO content leads to structures with less tetragonal characteristics shifting the phase composition toward nanodomain and/or rhombohedral structure. Concomitant to that, changes in the type of secondary phase content were observed. While for PZT-SKN ceramics with PbO deficit ZrO_2 was detected in the X-ray patterns, along with PbO excess, PbO appears as secondary phase.

Combining the results on structural changes in the PZT matrix with the observation of secondary phase it was concluded that the shift in phase content is caused by a shift in the Zr/Ti ratio of the PZT-SKN matrix.

Via the change in structural characteristics, the PbO content significantly influences dielectric properties and high field strain of ceramics and multilayer actuators. Most significant correlations are an increase in high field strain, an increase in permittivity of the poled materials and a decrease in dielectric losses along with lower PbO content. The mechanisms outlined show up in PZT-SKN ceramics as well as in multilayer actuators. However, for a complete understanding of the latter, additional effects emerging from interaction between ceramic and electrode material during co-firing have to be taken into account.

Acknowledgements

The support of this project within the framework of the Collaborative Research Center "Electric Fatigue in Functional Materials" and grant HI 1867/1 – 1 by the DFG is gratefully acknowledged. The authors would also like to thank Antonio Cervelino from SLS Villigen for his support at the MS beamline and Jürgen Roedel, Carsten Albe and Yuri Genenko for fruitful discussions.

Figures:

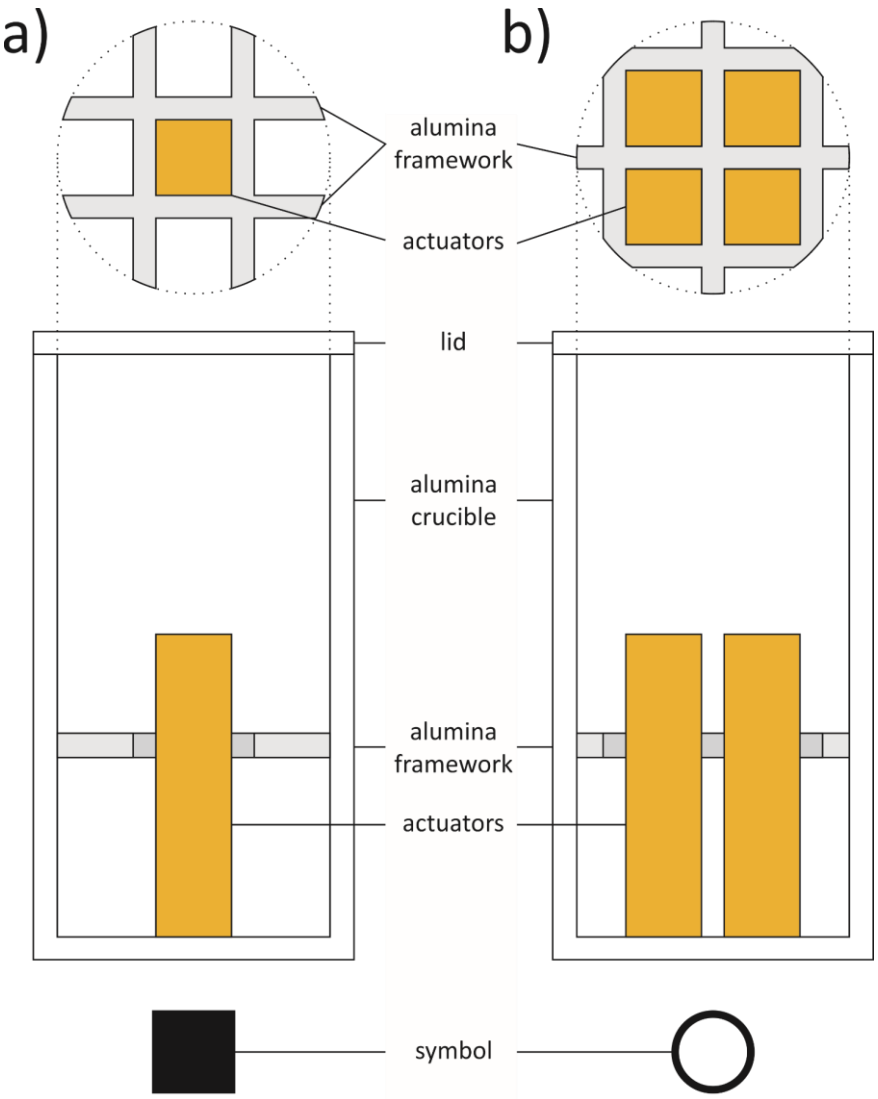

Figure 1: Sketch of the sintering setups for the PZT-SKN Multilayer actuators showing the crucible loaded with actuators in side view and top view a) one actuator arranged in the center of the crucible and b) four actuators in the crucible.

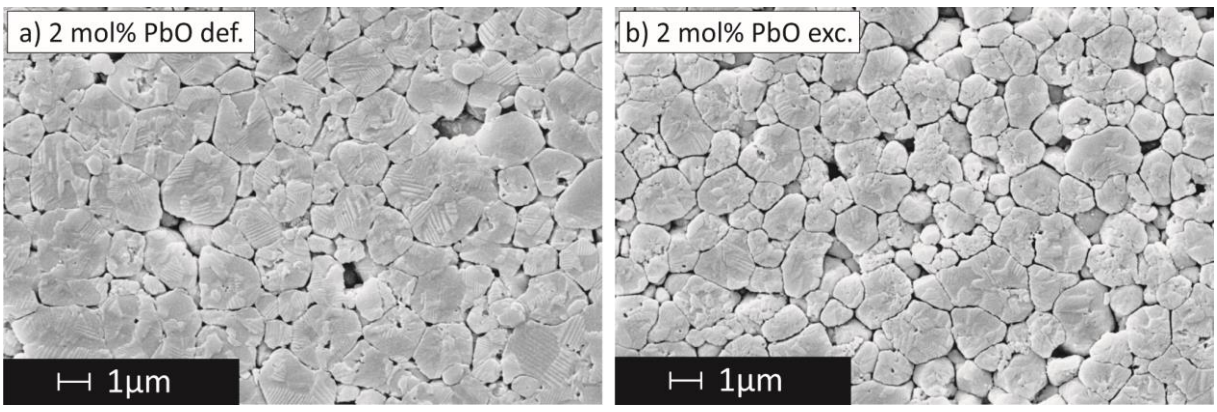

Figure 2: Microstructure of PZT-SKN ceramics with a) 2 mol% PbO deficit vs. b) PZT-SKN ceramics with 2 mol% PbO excess, both sintered at 1050°C/6 h.

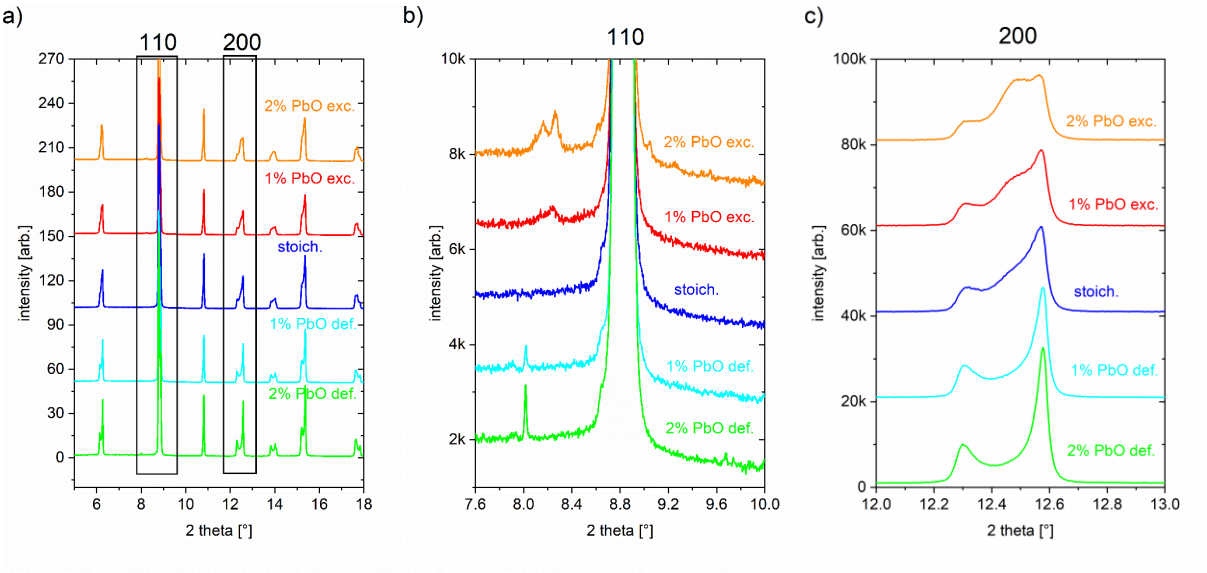

Figure 3: X-ray diffraction patterns of PZT-SKN recorded at the SLS (λ = 0.44304 Å) a) full pattern, b) angular region with ZrO_2 and lead oxide secondary phase peaks, c) angular range with PZT 200 reflections.

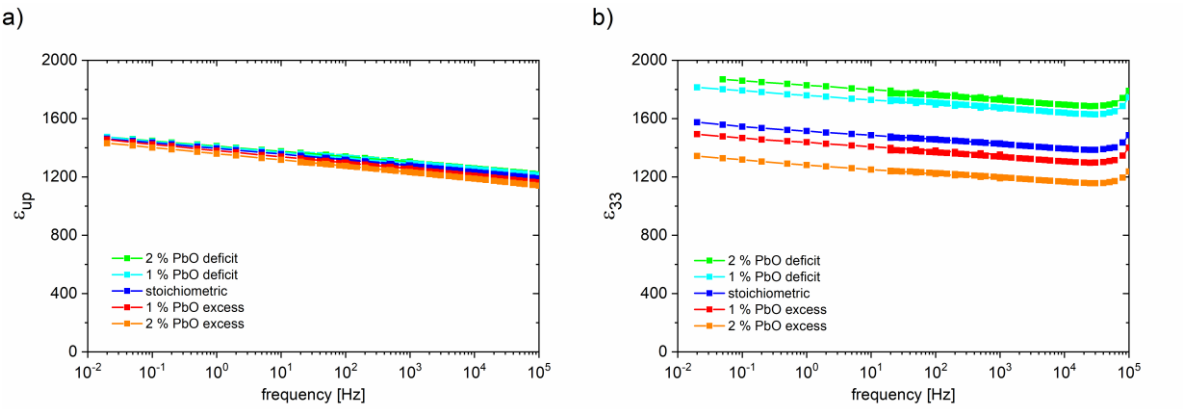

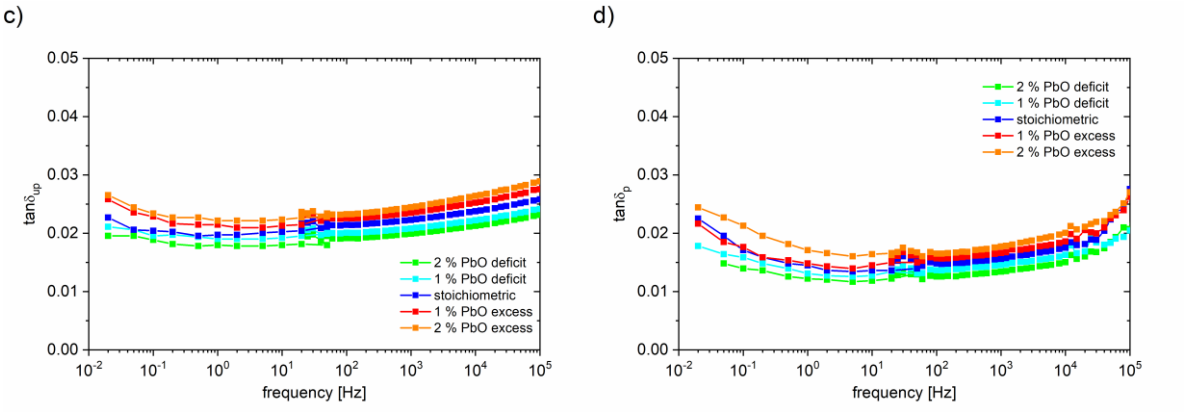

Figure 4: Dielectric characteristics of PZT-SKN with varying PbO-stoichiometry: a) relative permittivity unpoled, b) relative permittivity poled state, c) dielectric losses unpoled and d) dielectric losses poled state.

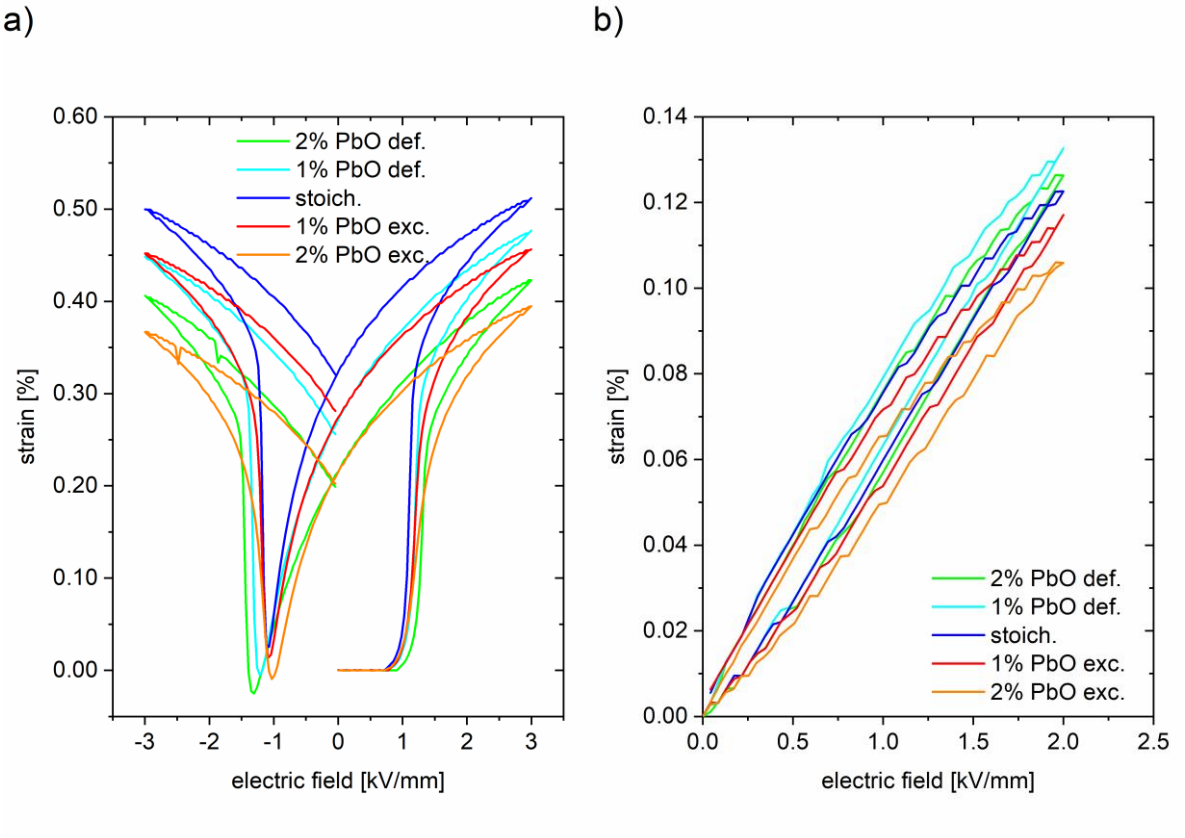

Figure 5: Strain of PZT-SKN ceramics under high electric fields: a) remanent strain and b) unipolar strain.

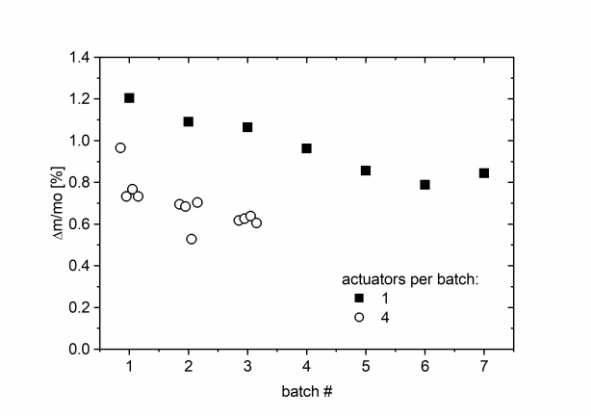

Figure 6: Sintering mass losses of PZT-SKN multilayer actuators under different sintering set-ups.

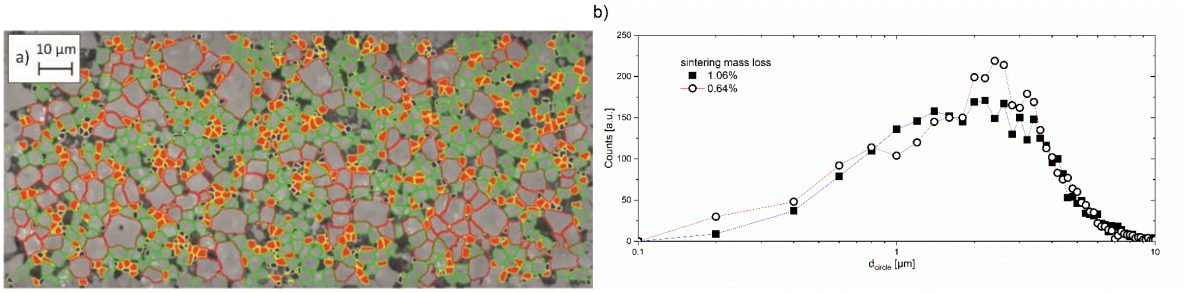

Figure 7: a) Microstructure imaging analysis and b) grain size distribution for PZT-SKN multilayer actuators, sintered under different setups resulting in differences in sintering mass losses.

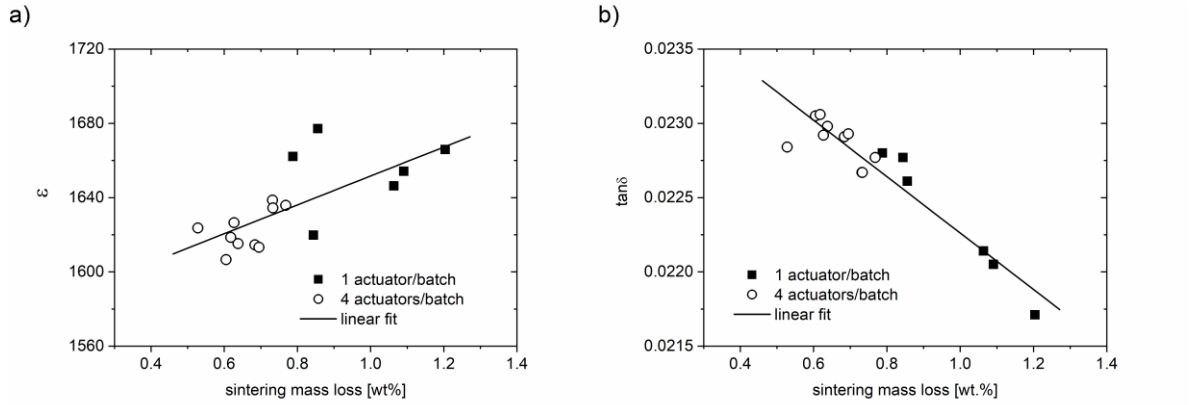

Figure 8: Dielectric properties of PZT-SKN multilayer actuators depending on their sintering

mass losses a) relative permittivities and b) dielectric losses.

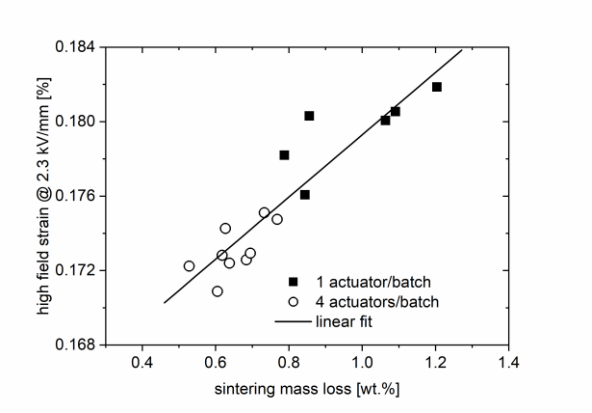

Figure 9: Field induced strain of PZT-SKN multilayer actuators depending on their sintering mass losses.

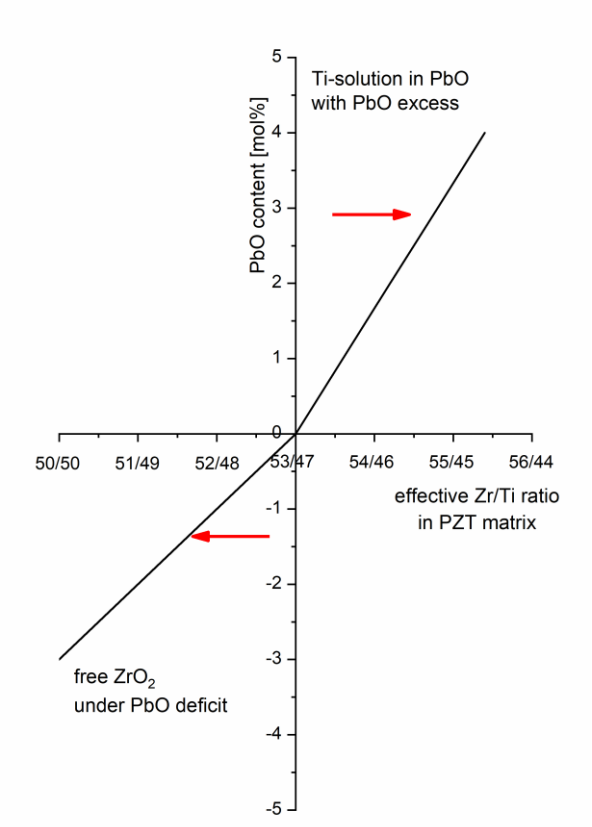

Figure 10: Shift in chemical composition (Zr/Ti-ratio) with PbO content (schematical diagram, Zr/Ti ratios and PbO contents are only for illustration, no quantitative relations are suggested).

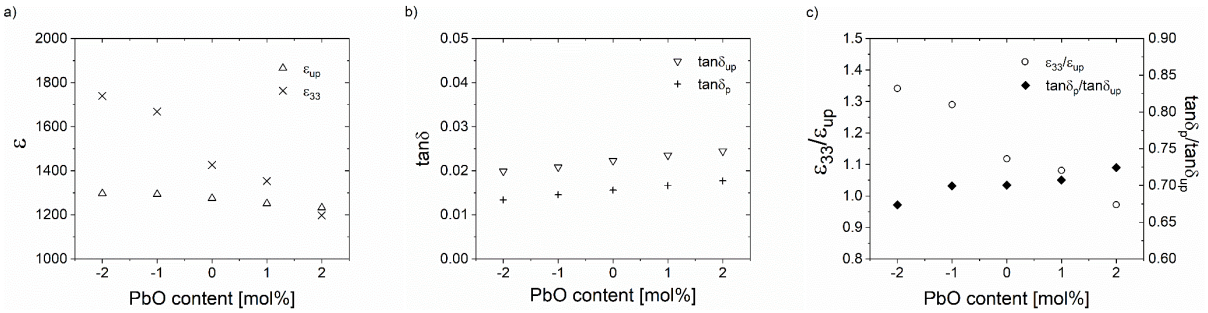

Figure 11: Summary of dielectric data at 1 kHz related to the PbO content of the PZT-SKN ceramics. a) Relative permittivities in unpoled state (ε) and in poled state (ε_{33}), b) dielectric losses tanδ in unpoled and poled state and c) ratios of permittivities and dielectric losses of the poled and unpoled state.

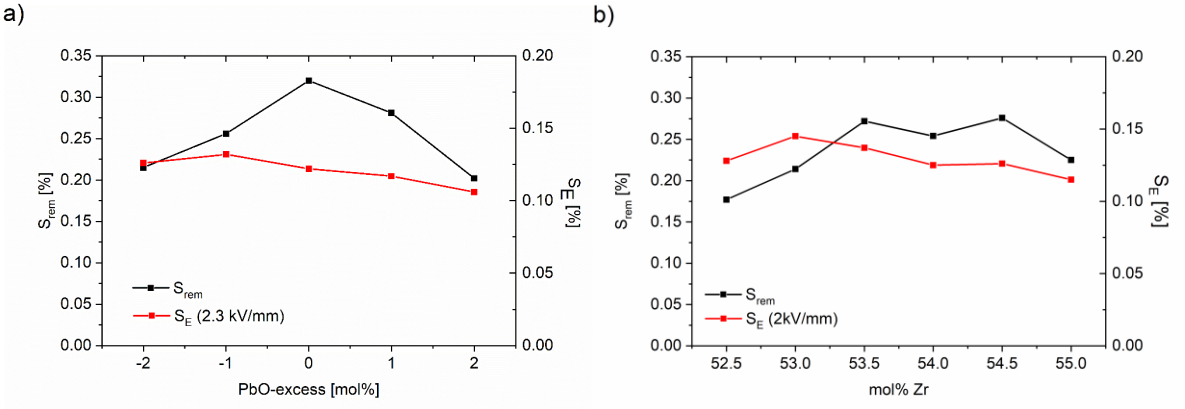

Figure 12: High field strain data change a) depending on PbO content in PZT-SKN under constant Zr/Ti and b) depending on Zr/Ti-content for stoichiometric PZT-1La2Sr(26).

Tables:

Table 1: Sintering mass losses and densities of the PZT-SKN ceramics depending on their PbO-stoichiometry as determined for three pellets for each composition.

	-2% PbO deficit	-1% PbO deficit	stoichiometric	1% PbO excess	2% PbO excess
	0.04	0.07	0.13	0.43	0.87

sintering mass loss [wt.%]	0.08	0.06	0.13	0.41	0.86
	0.06	0.07	0.14	0.42	0.86
density [g/cm^3]	7.77	7.75	7.82	7.81	7.76
	7.79	7.79	7.83	7.83	7.74
	7.78	7.81	7.82	7.83	7.77

Table 2: Parameters and correlation coefficients for the linear fits ($f(x) = a + b * x$) on dielectric properties and field induced strain vs. sintering mass losses of multilayer actuators.

correlation (vs. sintering mass loss)	regression coefficient *a*	regression coefficient *b*	correlation coefficient ρ
relative permittivities ε	1573.9	77.76	0.70
dielectric losses tanδ	0.0246	-0.0019	-0.94
high field strain S_E	0.1625	0.0167	0.92

Table 3: Lead oxide contents, sintering mass losses and remaining, real PbO content in the PZT-SKN ceramics.

intended PbO-stoichiometry [mol%]	sintering mass loss [wt.%]	real PbO stoichiometry [mol%]
-2.0	0.06	-2.09
-1.0	0.07	-1.10
0.0	0.14	-0.20
1.0	0.42	0.39
2.0	0.86	0.75

1. Haertling GH. Ferroelectric Ceramics: History and Technology. J Am Ceram Soc [Internet]. 1999 Apr 21 [cited 2014 Oct 27];82(4):797–818. Available from: http://doi.wiley.com/10.1111/j.1151-2916.1999.tb01840.x

2. Holman RL, Fulrath RM. Intrinsic nonstoichiometry in the lead zirconate-lead titanate system determined by Knudsen effusion. J Appl Phys [Internet]. 1973 Dec;44(12):5227–36. Available from: http://aip.scitation.org/doi/10.1063/1.1662136

3. Kingon AI, Clark JB. Sintering of PZT Ceramics: I, Atmosphere Control. J Am Ceram Soc [Internet]. 1983 Apr;66(4):253–6. Available from: http://doi.wiley.com/10.1111/j.1151-2916.1983.tb15708.x

4. Kingon AI, Clark JB. Sintering of PZT Ceramics: II, Effect of PbO Content on Densification Kinetics. J Am Ceram Soc [Internet]. 1983 Apr;66(4):256–60. Available from: http://doi.wiley.com/10.1111/j.1151-2916.1983.tb15709.x

5. Chiang S-S, Nishioka M, Fulrath RM, Pask JA. Effects of processing on microstructure and properties of PZT ceramics. Ceram Bull. 1981;60(September):484–9.

6. Smyth DM. Defect structure in perovskite titanates. Curr Opin Solid State Mater Sci [Internet]. 1996 Oct;1(5):692–7. Available from: http://www.sciencedirect.com/science/article/pii/S1359028696800532

7. Donnelly NJ, Randall CA. Impedance spectroscopy of PZT ceramics- measuring diffusion coefficients, mixed conduction, and Pb loss. IEEE Trans Ultrason Ferroelectr Freq Control [Internet]. 2012 Sep;59(9):1883–7. Available from: http://ieeexplore.ieee.org/document/6306003/

8. Gesemann R, Neels H. Einige Probleme der Bildung von $Pb(ZrTi)O_3$ - Mischkristallen. Hermsdorfer Tech Mitteilungen. 1965;12:339–42.

9. Haerdtl KH, Rau H. PbO-vapour pressure in the $Pb(Ti_{1-x}Zr_x)O_3$ System. Solid State Commun. 1969;7:41–5.

10. Holman RL. Novel uses of the thermo-microbalance in the determination of nonstoichiometry in complex oxide systems. J Vac Sci Technol [Internet]. 1974 Jan;11(1):434–9. Available from: http://avs.scitation.org/doi/10.1116/1.1318649

11. Schulze WA, Miller TG, Biggers J V. Solubility Limit of La in the Lead Zirconate-Titanate System. J Am Ceram Soc [Internet]. 1975 Jan;58(1–2):21–3. Available from: http://doi.wiley.com/10.1111/j.1151-2916.1975.tb18973.x

12. Hammer M, Hoffmann MJ. Sintering Model for Mixed-Oxide-Derived Lead Zirconate Titanate Ceramics. J Am Ceram Soc [Internet]. 1998 Dec [cited 2011 Sep 29];81(12):3277–84. Available from: http://doi.wiley.com/10.1111/j.1151-2916.1998.tb02768.x

13. Kishi H, Mizuno Y, Chazono H. Base-Metal Electrode-Multilayer Ceramic Capacitors: Past, Present and Future Perspectives. Jpn J Appl Phys [Internet]. 2003 Jan 15;42(Part 1, No. 1):1–15. Available from: http://stacks.iop.org/1347-4065/42/1

14. Randall CA, Kelnberger A, Yang GY, Eitel RE, Shrout TR. High Strain Piezoelectric Multilayer Actuators-A Material Science and Engineering Challenge. J Electroceramics [Internet]. 2005 Jul [cited 2014 Feb 20];14(3):177–91. Available from: http://link.springer.com/10.1007/s10832-005-0956-5

15. Uchino K. Multilayer Technologies for Piezoceramic Materials. In: Advanced Piezoelectric Materials [Internet]. Elsevier; 2017. p. 423–51. Available from: http://linkinghub.elsevier.com/retrieve/pii/B9780081021354000114

16. Laurent M. Untersuchung der Wechselwirkungen zwischen Keramik und Elektroden beim Kosintern von PZT-Vielschichtaktoren mit Ag/Pd-Elektroden. Universität Karlsruhe; 2002.

17. Marincel DM, Jesse S, Belianinov A, Okatan MB, Kalinin S V., Jackson TN, et al. A-site stoichiometry and piezoelectric response in thin film $PbZr_{1-x}Ti_xO_3$. J Appl Phys

[Internet]. 2015 May 28;117(20):204104. Available from: http://aip.scitation.org/doi/10.1063/1.4921869

18. Jaffe B, Cook WR, Jaffe H. Piezoelectric Ceramics. London: Academic Press; 1971.

19. Helke G, Lubitz K. Piezoelectric PZT Ceramics. In: Piezoelectricity [Internet]. Berlin, Heidelberg: Springer Berlin Heidelberg; p. 89–130. Available from: http://link.springer.com/10.1007/978-3-540-68683-5_4

20. Raymond MV, Smyth DM. Defects and charge transport in perovskite ferroelectrics. J Phys Chem Solids [Internet]. 1996 Oct;57(10):1507–11. Available from: http://linkinghub.elsevier.com/retrieve/pii/0022369796000200

21. Ikeda T, Okano T, Watanabe M. A Ternary System PbO-TiO_2-ZrO_2. Jpn J Appl Phys [Internet]. 1962 Apr;1(4):218–22. Available from: http://stacks.iop.org/1347-4065/1/218

22. Fushimi S, Ikeda T. Phase Equilibrium in the System PbO-TiO_2-ZrO_2. J Am Ceram Soc. 1967;50(3):129–32.

23. Helke G, Seifert S, Cho S-J. Phenomenological and structural properties of piezoelectric ceramics based on xPb(Zr,Ti) O_3-(1-x)Sr($K_{0.25}Nb_{0.75}$)O_3 (PZT/SKN) solid solutions. J Eur Ceram Soc [Internet]. 1999 Jun;19(6–7):1265–8. Available from: http://www.sciencedirect.com/science/article/pii/S0955221998004178

24. Patterson BD, Brönnimann C, Maden D, Gozzo F, Groso A, Schmitt B, et al. The materials science beamline at the Swiss Light Source. In: Nuclear Instruments and Methods in Physics Research, Section B: Beam Interactions with Materials and Atoms [Internet]. 2005 [cited 2011 Feb 21]. p. 224–8. Available from:

http://linkinghub.elsevier.com/retrieve/pii/S016890020402412X

25. Bergamaschi A, Cervellino A, Dinapoli R, Gozzo F, Henrich B, Johnson I, et al. Photon counting microstrip detector for time resolved powder diffraction experiments. Nucl Instruments Methods Phys Res Sect A Accel Spectrometers, Detect Assoc Equip [Internet]. 2009 Jun;604(1–2):136–9. Available from: http://linkinghub.elsevier.com/retrieve/pii/S0168900209001351

26. Kungl H, Fett T, Wagner S, Hoffmann MJ. Nonlinearity of strain and strain hysteresis in morphotropic LaSr-doped lead zirconate titanate under unipolar cycling with high electric fields. J Appl Phys [Internet]. 2007 Feb 15;101(4):044101. Available from: http://aip.scitation.org/doi/10.1063/1.2434836

27. Kungl H, Hoffmann MJ. Method for the estimation of the total displacement of ferroelectric actuators under mixed thermal and electrical loading. Sensors Actuators A Phys [Internet]. 2008 Jun;144(2):328–36. Available from: http://linkinghub.elsevier.com/retrieve/pii/S092442470800085X

28. Bindig R, Schreiner HJ. Piezoceramic multi-layer element [Internet]. Google Patents; US 9598319 B2, 2008. Available from: http://www.google.sr/patents/US9598319

29. Oldenkotte M. Einfluß der Sinteratmosphäre auf die Eigenschaften kogesinterter PZT-Multilayeraktoren mit Ag-Pd Elektroden. Karlsruhe Institute of Technology; 2013.

30. Schoenau KA, Schmitt LA, Knapp M, Fuess H, Eichel R-A, Kungl H, et al. Nanodomain structure of Pb[Zr_{1−x}Ti_{x}]O_{3} at its morphotropic phase boundary: Investigations from local to average structure. Phys Rev B [Internet]. 2007 May [cited 2011 Feb 15];75(18):184117. Available from:

http://link.aps.org/doi/10.1103/PhysRevB.75.184117

31. Schmitt LA, Schoenau KA, Theissmann R, Fuess H, Kungl H, Hoffmann MJ. Composition dependence of the domain configuration and size in Pb(Zr[sub 1−x]Ti[sub x])O[sub 3] ceramics. J Appl Phys [Internet]. 2007 [cited 2011 Feb 21];101(7):74107. Available from: http://link.aip.org/link/JAPIAU/v101/i7/p074107/s1&Agg=doi

32. Noheda B, Cox DE, Shirane G. Stability of the monoclinic phase in the ferroelectric perovskite PbZr_{1-x}Ti_{x}O_{3}. Phys Rev B [Internet]. 2000 Dec [cited 2011 Feb 4];63(1):1–9. Available from: http://link.aps.org/doi/10.1103/PhysRevB.63.014103

33. Donnelly NJ, Shrout TR, Randall CA. Addition of a Sr, K, Nb (SKN) Combination to PZT(53/47) for High Strain Applications. J Am Ceram Soc [Internet]. 2007 Feb;90(2):490–5. Available from: http://doi.wiley.com/10.1111/j.1551-2916.2006.01450.x

34. Erdem E, Eichel R-A, Kungl H, Hoffmann MJ, Ozarowski A, van Tol J, et al. Characterization of (FeZr,Ti-Vo ldrldr)ldr defect dipoles in (La,Fe)-codoped PZT 52.5/47.5 piezoelectric ceramics by multifrequency electron paramagnetic resonance spectroscopy. IEEE Trans Ultrason Ferroelectr Freq Control [Internet]. 2008 May;55(5):1061–8. Available from: http://ieeexplore.ieee.org/document/4524985/

35. Eichel R-A, Kungl H, Jakes P. Defect structure of non-stoichiometric and aliovalently doped perovskite oxides. Mater Technol [Internet]. 2013 Sep 18;28(5):241–6. Available from: http://www.tandfonline.com/doi/full/10.1179/175355513X13715615193120

36. Takahashi S. Effects of impurity doping in lead zirconate-titanate ceramics.

Ferroelectrics [Internet]. 1982 May 7;41(1):143–56. Available from: http://www.tandfonline.com/doi/abs/10.1080/00150198208210617

37. Randall CA, Kim N, Kucera J, Cao W, Shrout TR. Intrinsic and Extrinsic Size Effects in Fine-Grained Morphotropic-Phase-Boundary Lead Zirconate Titanate Ceramics. J Am Ceram Soc [Internet]. 2005 Jan [cited 2011 Feb 23];81(3):677–88. Available from: http://doi.wiley.com/10.1111/j.1151-2916.1998.tb02389.x

38. Kungl H, Hoffmann MJ. Effects of sintering temperature on microstructure and high field strain of niobium-strontium doped morphotropic lead zirconate titanate. J Appl Phys [Internet]. 2010 [cited 2011 Jul 13];107(5):054111. Available from: http://link.aip.org/link/JAPIAU/v107/i5/p054111/s1&Agg=doi

39. Sakaki C, Newalkar BL, Komarneni S, Uchino K. Grain Size Dependence of High Power Piezoelectric Characteristics in Nb Doped Lead Zirconate Titanate Oxide Ceramics. Jpn J Appl Phys [Internet]. 2001 Dec 15;40(Part 1, No. 12):6907–10. Available from: http://stacks.iop.org/1347-4065/40/6907

40. Kakegawa K, Matsunaga O, Kato T, Sasaki Y. Compositional Change and Compositional Fluctuation in Pb(Zr,Ti)O3 Containing Excess PbO. J Am Ceram Soc [Internet]. 1995 Apr;78(4):1071–5. Available from: http://doi.wiley.com/10.1111/j.1151-2916.1995.tb08439.x

41. Turik A V., Kupriyanov MF, Sidorenko EN, Zaitsev SM. Behavior of piezoceramics of type $Pb(Zr_xTi_{1-x})O_3$ near the reagion of morphotropic transition. Sov Phys Tech Phys. 1980;25(10):1251–4.

42. Saito Y, Takao H. High Performance Lead-free Piezoelectric Ceramics in the

(K,Na)NbO_3-$LiTaO_3$ Solid Solution System. Ferroelectrics [Internet]. 2006 Aug 10;338(1):17–32. Available from: https://www.tandfonline.com/doi/full/10.1080/00150190600732512

43. Wagner S, Kahraman D, Kungl H, Hoffmann MJ, Schuh C, Lubitz K, et al. Effect of temperature on grain size, phase composition, and electrical properties in the relaxor-ferroelectric-system $Pb(Ni_{1/3}Nb_{2/3})O_3$-$Pb(Zr,Ti)O_3$. J Appl Phys [Internet]. 2005 Jul 15;98(2):024102. Available from: http://aip.scitation.org/doi/10.1063/1.1968427

44. Kungl H, Theissmann R, Knapp M, Baehtz C, Fuess H, Wagner S, et al. Estimation of strain from piezoelectric effect and domain switching in morphotropic PZT by combined analysis of macroscopic strain measurements and synchrotron X-ray data. Acta Mater [Internet]. 2007 Apr [cited 2011 Aug 12];55(6):1849–61. Available from: http://linkinghub.elsevier.com/retrieve/pii/S1359645406007841

45. Webster AH, Weston TB, Bright NFH. Effect of PbO Deficiency on the Piezoelectric Properties of Lead Zirconate-Titanate Ceramics. J Am Ceram Soc [Internet]. 1967 Sep;50(9):490–1. Available from: http://doi.wiley.com/10.1111/j.1151-2916.1967.tb15170.x

46. Setter N. Piezoelectric materials in devices: extended reviews on current and emerging piezoelectric materials, technology, and applications. 2002. 518 p.

47. Nicolai M, Eßlinger S, Schönecker A. Identification of process parameters for efficient poling of PZT ceramics for mass production. J Electroceramics [Internet]. 2014 May 27;32(2–3):180–6. Available from: http://link.springer.com/10.1007/s10832-013-9866-0